

# ***Ab Initio* Study on Electronic Structure of ZrB<sub>12</sub> under High Hydrostatic Pressure**

Z. F. Hou

*Department of Physics, Fudan University, Shanghai, P. R. China 200433\**

(Dated: October 18, 2018)

## **Abstract**

Using projector augmented wave approach within the generalized gradient approximation, we have studied the structural property and electronic structure of ZrB<sub>12</sub>. The calculated lattice constants and bulk modulus are in good agreement with the available experimental values. A detailed study of the electronic structure and the charge-density redistribution reveals the features of strong covalent B-B and weak covalent Zr-B bondings in ZrB<sub>12</sub>. The states at the Fermi level mainly come from the  $\sigma$ - $p_y$  and  $\pi$ - $p_z$  orbitals of boron atoms, which are slightly hybridized with the  $t_{2g}$ - $d_{xz}$  and  $t_{2g}$ - $d_{yz}$  orbitals of Zr atoms. As the increased hydrostatic pressure on ZrB<sub>12</sub>, the total density of states at the Fermi level decreases.

---

\*Electronic address: zhou@fudan.edu.cn

## I. INTRODUCTION

Metal borides have been the subject of extensive research in recent years [1, 2, 3] because they exhibit unique properties such as high melting points, high hardness values, and excellent oxidation resistance. These particular properties mean borides are promising materials for new heat-resistant, corrosion-resistant, and wear-resistant alloys and coatings [4]. In particular, the discovery of superconductivity ( $T_C \sim 39$  K) in magnesium diboride ( $\text{MgB}_2$ ) [5], which is crystallized in a simple layered hexagonal  $\text{AlB}_2$  structure, has stimulated a renewed interest to search for new superconductors and to understand their mechanism of superconductivity in borides.

$\text{ZrB}_{12}$  is found to have the highest superconductivity critical temperature ( $T_C \sim 6$  K) in the family of dodecaborides  $MB_{12}$  [6, 7, 8]. In order to understand its superconductivity, some efforts are made by measuring the specific heat, magnetic susceptibility, resistivity, thermal expansion, electron transport, penetration depth, and the upper critical magnetic field of  $\text{ZrB}_{12}$  [7, 8, 9, 10, 11, 12, 13, 14, 15, 16]. Specially, a negative pressure effect on  $T_C$  of  $\text{ZrB}_{12}$  is observed in its magnetization measurements under pressure, which contrasts to the previous suggestion that the superconducting critical temperature of  $\text{ZrB}_{12}$  might increase under pressure [17]. The previous band structure calculations on  $\text{ZrB}_{12}$  mainly concern the electronic structure of  $\text{ZrB}_{12}$  under ambient pressure [18, 19]. Therefore, we perform *ab initio* total energy calculations to study the properties of  $\text{ZrB}_{12}$ , especially about its electronic structure under high pressure.

## II. METHOD

All calculations on  $\text{ZrB}_{12}$  are performed using the projector augmented wave (PAW) approach as implemented in the VASP code [20, 21]. The exchange-correlation energy functional is treated with the generalized gradient approximation (GGA) with Perdew and Wang parameterization (known as GGA-PW91) [22]. Electron-ion interaction is represented by the PAW method [23, 24] and wave functions are expanded by the plane waves up to an energy cutoff of 500 eV. Brillouin-zone integrations are approximated using the special  $k$ -point sampling of Monkhorst-Pack scheme [25] with a  $9 \times 9 \times 9$  grid. The above calculation parameters of energy cutoff and  $k$ -mesh make the total energy convergence to 2 meV/atom.

The internal atomic coordinates of cubic  $\text{ZrB}_{12}$  are relaxed at a series of fixed volumes until the force exerting on each atom is less than  $0.01 \text{ eV}/\text{\AA}$ . The obtained energies are fitted with the third-order Birch-Murnaghan equation of state (EOS) [26] to give the equilibrium volume and the minimum energy. The final calculated cell parameters are listed in Table I.

### III. RESULTS AND DISCUSSIONS

The crystalline structure of  $\text{ZrB}_{12}$  is cubic and belongs to space group  $\text{O}_h^5\text{-}Fm\bar{3}m$  (No.225) [27], shown in Fig. 1. The Wyckoff positions of Zr and boron atoms are  $4a$   $(0, 0, 0)$  and  $48i$   $(1/2, x, x)$ , respectively, i.e. the Zr atoms and cuboctahedral  $\text{B}_{12}$  clusters are arranged as in the  $\text{NaCl}$ -like structure. The 13-atom fcc unit cell of cubic  $\text{ZrB}_{12}$  is characterized by single lattice constant and the internal parameter of boron atoms. In present work, we obtain the lattice constant  $a$  is  $7.409 \text{ \AA}$  and the internal coordinate parameter  $x$  of boron atoms is 0.161, in good agreement with experiment values [27, 28] (See Table I). Based on GGA calculations, the bulk modulus and its pressure derivative for  $\text{ZrB}_{12}$  are predicted as 233.0 GPa and 3.64, respectively. Note that in the investigation of electron-phonon coupling dependent on pressure of  $\text{ZrB}_{12}$  the authors [9] used the bulk modulus of an analogy compound  $\text{UB}_{12}$  ( $B_0 = 249 \text{ GPa}$ ) because the experimental value of bulk modulus of  $\text{ZrB}_{12}$  is not reported. In addition, the predicted bulk modulus of  $\text{ZrB}_{12}$  is close to that of  $\text{ZrB}_2$  (245 GPa obtained from the ultrasonic measurements [29] or 238 GPa predicted from *ab initio* calculations [30]) crystallized in hexagonal layered  $\text{AlB}_2$ -like structure.

The energy band structure and electronic density of states (DOS) of cubic  $\text{ZrB}_{12}$  in equilibrium are shown in Fig. 2(a) and 3, respectively. These may be compared well with previously calculated results of  $\text{ZrB}_{12}$  based on a variety of computational methods [18, 19]. Overall these suggest that  $\text{ZrB}_{12}$  exhibits a metallic character with the mixed  $p$ - $d$  states rather than a simple  $p$ - or  $d$ -metal [9]. The valence bands in Fig. 2(a) are split into three disjointed groups. The lowest group centered at -15 eV below the Fermi level ( $E_F$ ) has a width of about 1 eV and the corresponding bands mostly come from the bonding states of B- $2s$  orbitals. Combining from the DOS figures (3), the higher one in the energy range from -13 eV to -10 eV below the  $E_F$  is largely contributed by the antibonding states of B- $2s$  orbitals. The upper one in the energy range from -10 eV to  $E_F$  is mainly composed by B- $2p$  orbitals and Zr- $4d$  electrons. In addition, it suggests that there is a weak hybridization

between B-2p and Zr-4d orbitals occurring below the  $E_F$ . The total density of states at the Fermi level  $N(E_F)$  is about 1.478 states/eV·unit cell, in consistence with the calculated value in other work [18]. The states at  $E_F$  is mainly made by the 2p electrons of boron atoms ( $\sigma$ - $p_y$  and  $\pi$ - $p_z$  orbitals) and 4d levels of Zr atom ( $t_{2g}$ - $d_{yz}$  and  $t_{2g}$ - $d_{xz}$  orbitals). This can also be seen from the the partial charge density calculated within a 0.2 eV energy window around  $E_F$  for  $\text{ZrB}_{12}$ , which is shown in Fig. 4(b).

In order to understand the Zr-B and B-B bondings of  $\text{ZrB}_{12}$  in equilibrium, the line charge density along nearest neighbor Zr–B and B–B pairs are illustrated in Fig. 5. The calculated bond lengths of atoms are  $d_{\text{Zr-B}} = 2.75 \text{ \AA}$  and  $d_{\text{B-B}} = 1.68 \text{ \AA}$ , which agree well with the experimental values [28]. It is clearly seen that charge highly accumulates around Zr atom due to its more valence electrons than that of boron atom. Contrast to the strong covalent character of B-B bonding, the Zr-B bonding exhibits a weak covalent character. It also supported by above discussion that the  $d$  orbital of Zr atoms and  $p$  orbital of boron atoms have a weak hybridization. In order to further reveal the topology of the Zr-B and B-B bondings, Fig. 4(b) illustrates the contour plots of electron density on crystallographic (010) plane. It again indicates that B-B bonding exhibits a strong covalent character.

Now we turn to discuss the effect of high hydrostatic pressure on electronic structure of  $\text{ZrB}_{12}$ . The values of DOS at the  $E_F$  for  $\text{ZrB}_{12}$  under a serial of hydrostatic pressure are listed in Table II. It can be seen that as the pressure increased from 0 to 22.1 GPa, the total density of states at the  $E_F$  decreases about 0.264 states/eV·unit cell. Considering the electron-phonon coupling constant  $\lambda_{\text{el-ph}}$  depends linearly on the  $N(E_F)$  [31], our calculated results indicate that the  $\lambda_{\text{el-ph}}$  of  $\text{ZrB}_{12}$  would decrease under the high pressure. It also supported by recent experimental observation [9] that there is a negative pressure effect on  $T_C$  and  $\lambda_{\text{el-ph}}$  of  $\text{ZrB}_{12}$  with  $dT_C/dp$  of -0.0225 K/kbar and  $d\ln\lambda_{\text{el-ph}}/dp$  of -0.2%/kbar. Additionally, as the hydrostatic pressure increased, the contribution to  $N(E_F)$  of Zr atoms decrease than that of boron atoms. This could be understood from that the B-B bonding is stronger than Zr-B bonding, and hence the bond length of B-B atoms decreases more slightly under the high pressure (see Table II). Upon the hydrostatic pressure to 22.1 GPa, the width of valence bands of  $\text{ZrB}_{12}$  is increased to -16 eV as shown in Fig. 2(b), companied with the 2s-bonding states of B boron atoms toward lower energy.

## IV. CONCLUSIONS

The structural property and electronic structure of  $\text{ZrB}_{12}$  have been calculated and analyzed. Our calculated structural parameters including the lattice constants and internal parameters are in good agreement with the experiment data. The detailed study of the electronic structure and charge density redistribution reveals the strong covalent of bonding of B-B atoms and role of  $p$  orbitals of boron atoms and  $d$  orbitals of Zr atom in the superconductivity of  $\text{ZrB}_{12}$ . Our calculated results also indicate that there is a negative pressure effect on the superconductivity of  $\text{ZrB}_{12}$ .

## V. ACKNOWLEDGEMENTS

The author acknowledges support from Shanghai Postdoctoral Science Foundation under Grant No. 05R214106. The computation was performed at Supercomputer Center of Fudan.

---

- [1] C. Buzea and T. Yamashita, *Supercond. Sci. Technol.* **14**, R115 (2001).
- [2] P. C. Canfield and S. L. Budko, *Phys. World* **15**, 29 (2002).
- [3] A. L. Ivanovskii, *Phys. Solid State* **45**, 1829 (2003).
- [4] T. Aizawa, S. Suehara, S. Hishita, and S. Otani, *Phys. Rev. B* **71** (2005).
- [5] J. Nagamatsu, N. Nakagawa, T. Muranaka, Y. Zenitani, and J. Akimitsu, *Nature* **401**, 63 (2001).
- [6] B. T. Matthias, T. H. Geballe, K. Andres, E. Corenzwit, G. W. Hull, and J. P. Maita, *Science* **159**, 530 (1968).
- [7] M. I. Tsindlekht, G. I. Leviev, I. Asulin, A. Shironi, O. Millo, I. Felner, Y. B. Paderno, V. B. Filippov, and M. A. Belogolovskii, *Phys. Rev. B* **69**, 212508 (2004).
- [8] R. Lortz, Y. Wang, S. Abe, C. Meingast, Y. B. Paderno, V. Filippov, and A. Junod, *Phys. Rev. B* **72**, 024547 (2005).
- [9] R. Khasanov, D. D. Castro, M. Belogolovskii, Y. Paderno, V. Filippov, R. Brutsch, and H. Keller, *Phys. Rev. B* **72**, 224509 (2005).
- [10] V. A. Gasparov, M. P. Kulakov, N. S. Sidorov, I. I. Zver'kova, V. B. Filipov, A. B. Lyashenko, and Y. B. Paderno, *Jetp Lett.* **80**, 330 (2004).

[11] V. A. Gasparov, N. S. Sidorov, I. I. Zver'kova, S. S. Khassanov, and M. P. Kulakov, *J. Exp. Theor. Phys.* **101**, 98 (2005).

[12] Y. Wang, R. Lortz, Y. Paderno, V. Filippov, S. Abe, U. Tutsch, and A. Junod, *Phys. Rev. B* **72**, 024548 (2005).

[13] G. I. Leviev, V. M. Genkin, M. I. Tsindlekht, I. Felner, Y. B. Paderno, and V. B. Filippov, *Phys. Rev. B* **71**, 064506 (2005).

[14] V. A. Gasparov, N. S. Sidorov, and I. I. Zver'kova, *Phys. Rev. B* **73**, 094510 (2006).

[15] M. I. Tsindlekht, G. I. Leviev, V. M. Genkin, I. Felner, Y. B. Paderno, and V. B. Filippov, *Phys. Rev. B* **73**, 104507 (2006).

[16] D. Daghero, R. S. Gonnelli, G. A. Ummarino, A. Calzolari, V. Dellarocca, V. A. Stepanov, V. B. Filippov, and Y. B. Paderno, *Supercond. Sci. Technol.* **17**, S250 (2004).

[17] Z. Fisk and B. T. Matthias, *Science* **165**, 279 (1969).

[18] I. R. Shein and A. L. Ivanovskii, *Phys. Solid State* **45**, 1429 (2003).

[19] B. Jäger, S. Paluch, O. J. Zogal, W. Wolf, P. Herzig, V. B. Filippov, N. Shitsevalova, and Y. Paderno, *J. Phys.: Condens. Matter* **17**, 2525 (2006).

[20] G. Kresse and J. Furthmüller, *Comput. Mater. Sci.* **6**, 15 (1996).

[21] G. Kresse and J. Furthmüller, *Phys. Rev. B* **54**, 11169 (1996).

[22] J. P. Perdew, J. A. Chevary, S. H. Vosko, K. A. Jackson, M. R. Pederson, D. J. Singh, and C. Fiolhais, *Phys. Rev. B* **46**, 6671 (1992).

[23] P. E. Blöchl, *Phys. Rev. B* **50**, 17953 (1994).

[24] G. Kresse and J. Joubert, *Phys. Rev. B* **50**, 1758 (1999).

[25] H. J. Monkhorst and J. D. Pack, *Phys. Rev. B* **13**, 5188 (1976).

[26] F. Birch, *Phys. Rev.* **71**, 809 (1947).

[27] Y. B. Kuzma, *Crystal Chemistry of Borides* (Vysshaya Shkola, Lvov, 1983).

[28] R. F. J. G. V. I. Matkovic, J. Economy and R. Barrett, *Acta Crystallogr.* **19**, 1056 (1965).

[29] N. L. Okamoto, M. Kusakari, K. Tanaka, H. Inui, M. Yamaguchi, and S. Otani, *J. Appl. Phys.* **93**, 88 (2003).

[30] V. Milman, B. Winkler, and M. I. J. Probert, *J. Phys.: Condens. Matter* **17**, 2233 (2005).

[31] W. L. McMillan, *Phys. Rev.* **167**, 331 (1968).

TABLE I: Calculated lattice parameter ( $a$ , in Å), atomic coordinate parameter ( $x$  for boron atoms), volumes of unit cell ( $V_0$ , in Å<sup>3</sup>), and bulk modulus ( $B_0$ , in GPa) of cubic ZrB<sub>12</sub>, along a comparison with other theoretical work and available experiment values.

	$a$	$x$	$V_0$	$B_0$
This work	7.409	0.1696	101.69	233.0
Other work [18]	7.419	-	102.09	-
Other work [19]	7.408	0.1696	102.09	-
Expt. [27]	7.408	0.166	101.63	-
Expt. [28]	7.408	0.1699	101.63	-

TABLE II: The bond lengths of atoms ( $d_{\text{Zr-B}}$  and  $d_{\text{B-B}}$ , in Å), total and partial density of states at the Fermi level ( $N(E_F)$  and  $N_{\text{par}}(E_F)$ , in states/eV·unit cell) of cubic ZrB<sub>12</sub> at different hydrostatic pressures.

Pressure	$d_{\text{Zr-B}}$	$d_{\text{B-B}}$	$N(E_F)$	$N_{\text{par}}(E_F)$	
				Zr-4d	B-2p
0 GPa	2.75	1.68	1.478	0.360	0.585
4.9 GPa	2.73	1.67	1.306	0.315	0.518
10.2 GPa	2.71	1.66	1.251	0.298	0.503
22.1 GPa	2.68	1.64	1.214	0.284	0.501

### Figure Captions

- FIG 1: The ball-and-stick model for unit cell of ZrB<sub>12</sub>. Zr atoms are shown as dark gray balls and boron atoms as light gray balls.
- FIG 2: Electronic band structure of ZrB<sub>12</sub> (a) in equilibrium and (b) at 22.1 GPa hydrostatic pressure. The zero of energy is set as the Fermi level and shown in dash line.
- FIG 3: (a) Total and partial density of states (DOS) , (b) and (c) angular momentum decompesed DOS of ZrB<sub>12</sub> in equilibrium.
- FIG 4: Contour plots of the charge density on (010) surface of ZrB<sub>12</sub> in equilibrium:

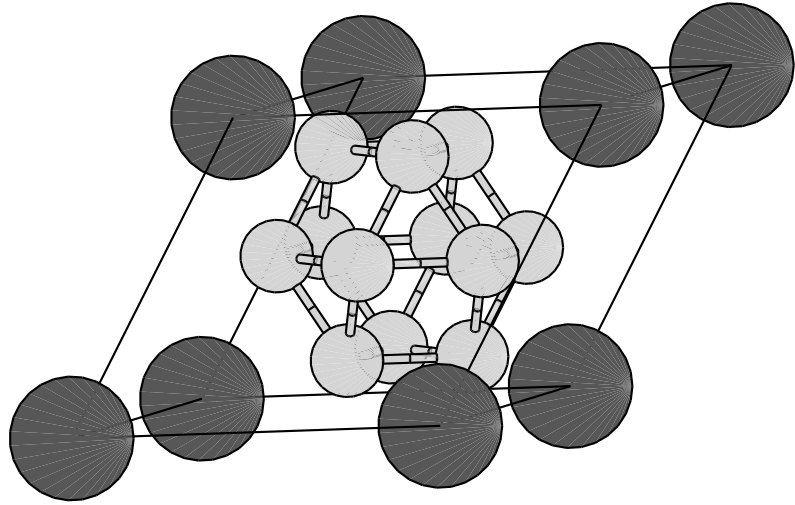


FIG. 1:

(a) partial charge density with the energy window of  $[E_F - 0.1, E_F + 0.1]$  is in an increment of  $2.0 \times 10^{-3} \text{ e}/\text{\AA}^3$  from 0 to  $2 \times 10^{-2} \text{ e}/\text{\AA}^3$  and (b) total charge density is in an increment of  $0.1 \text{ e}/\text{\AA}^3$  from 0 to  $1.5 \text{ e}/\text{\AA}^3$ .

- FIG 5: Charge density at the equilibrium lattice parameter of  $\text{ZrB}_{12}$ , along the lines strarting from: (a) Zr atom to nearest neighbor B atom, and (b) B atom to nearest neighbor B atom.

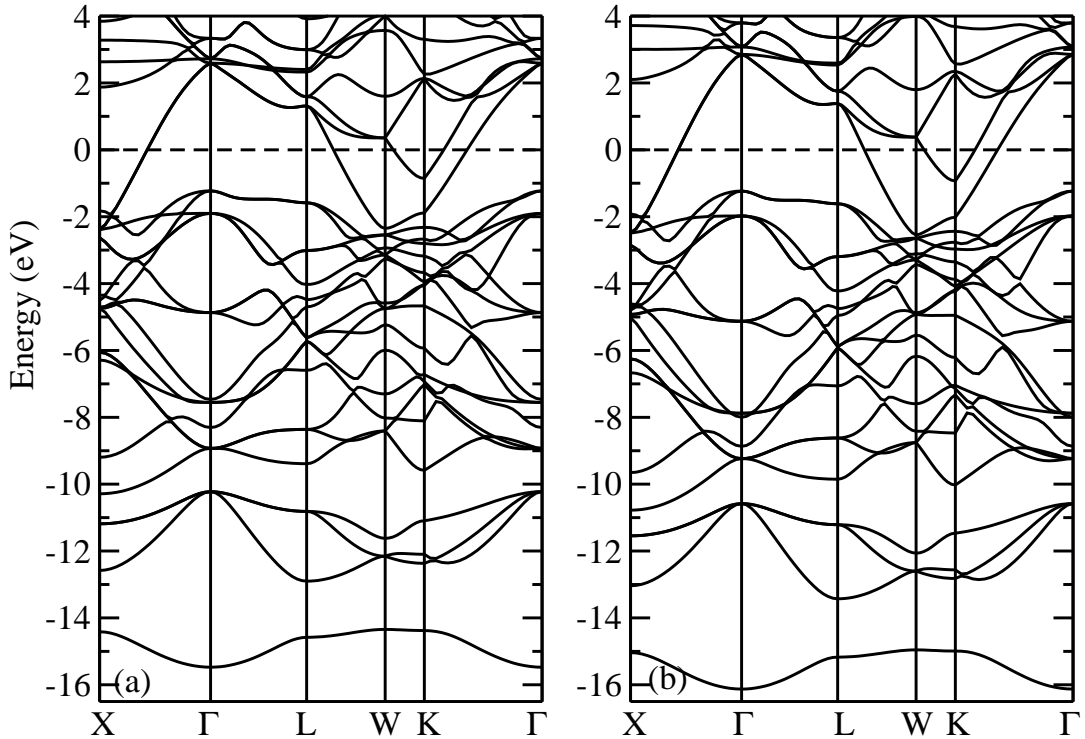


FIG. 2:

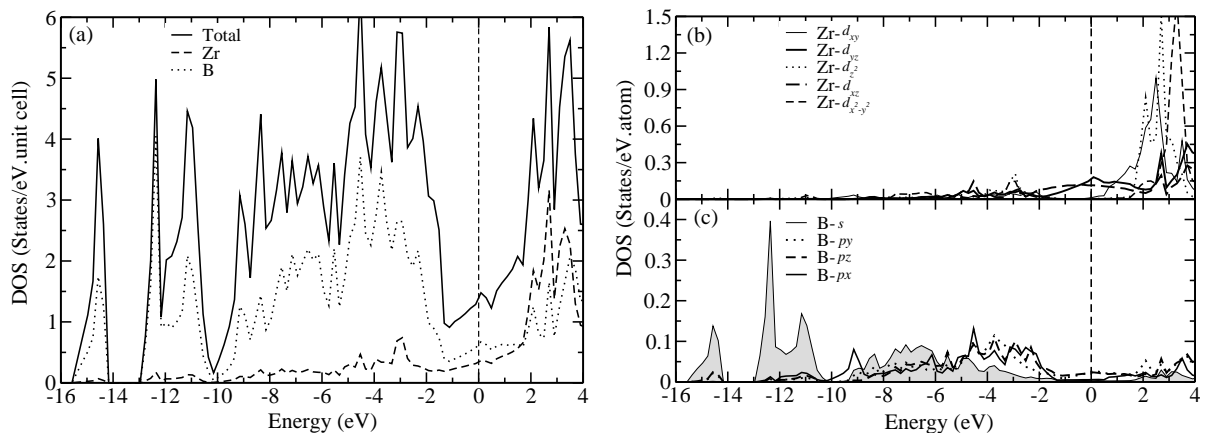


FIG. 3:

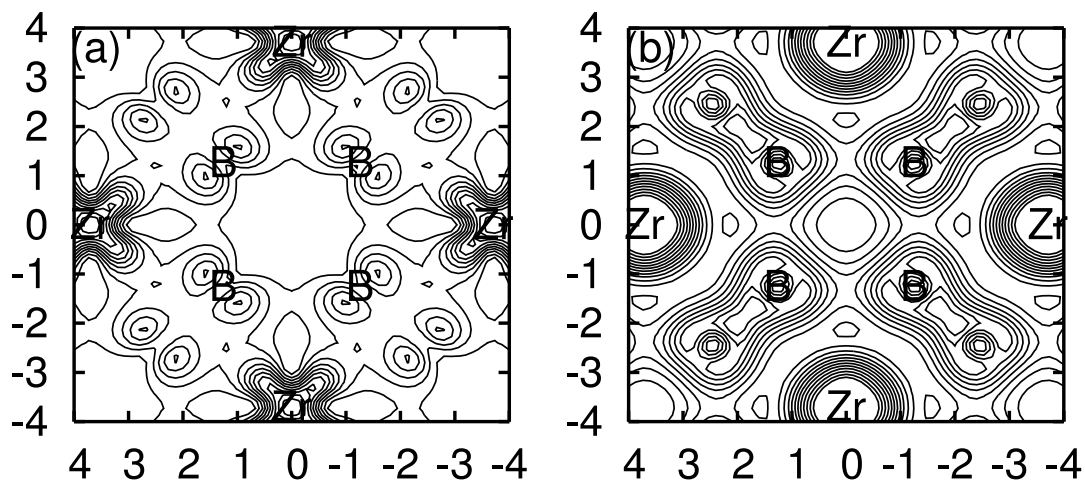


FIG. 4:

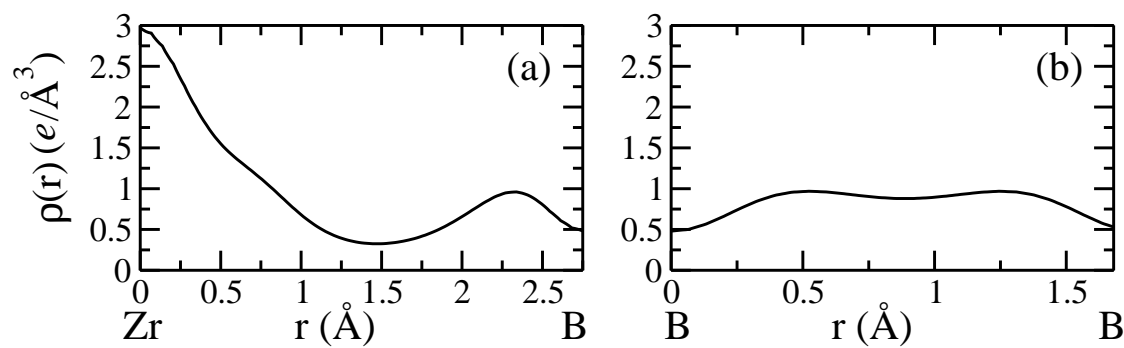


FIG. 5: